THE ASTROPHYSICAL JOURNAL, 415:L139–L142, 1993 October 1


# SHEAR IN THE IRAS 3282 OUTFLOW

M. TAFALLA,[1] R. BACHILLER,[2] J. MARTÍN-PINTADO,[2] AND M. C. H. WRIGHT[1]
*Received 1993 May 17; accepted 1993 July 14*

## ABSTRACT

We have observed with high resolution the ammonia emission around IRAS 3282, a young star with a highly collimated molecular outflow. Our data show the outflow, passing through the core, accelerates the dense gas and produces a shearlike velocity field. The acceleration occurs along the walls of a cavity which the outflow seems to have evacuated.

*Subject headings:* ISM: individual (IRAS 03282+3035) — ISM: jets and outflows — ISM: kinematics and dynamics — stars: formation

## 1. INTRODUCTION

Bipolar outflows can have a large impact on the cores where they occur. They often have kinetic energies comparable to the gravitational energies of the cores (Myers et al. 1988), and therefore have the potential to disperse the dense gas that surrounds young stellar objects (YSOs). Outflows, in fact, have become the most favored agents for ending protostellar accretion and driving the transition from embedded object to visible star (see, e.g., Shu, Adams, & Lizano 1987). Dense cores, on the other hand, affect the evolution of outflows. Cores probably do not collimate outflows, as they do not have enough potential energy and the collimation occurs at too small scales (see, e.g., Lada 1985) but, in some cases, they seem to perturb outflows by changing their direction and breaking the symmetry of the lobes (see, e.g., Umemoto et al. 1991). In addition, outflows consist mostly of swept-up gas (Snell 1987), so the cores at their centers must be an important source of molecular material. Bipolar outflows and star forming cores are therefore intimately coupled, interacting and evolving in a complex manner that is not yet well understood.

Highly collimated outflows are of particular interest in studying the outflow-core interplay. The fact they can maintain their collimation for large distances (tenths of parsecs) may suggest these outflows lie in privileged environments where they can flow without impediment. Or it could be that the collimation is intrinsic to youth, as the highly collimated outflows seem powered by "extreme Class I" sources (Bachiller & Gómez-González 1992). In this case, there must be a systematic decrease in outflow collimation with age, as no highly collimated outflows are associated with more evolved YSOs. The study of the dense gas around highly collimated outflows should therefore provide information on the first stages of the outflow-core interaction and on the evolution of outflow collimation.

In this paper we study the distribution of dense gas around the highly collimated outflow IRAS 3282. Discovered by Bachiller, Martín-Pintado, & Planesas (1991, hereafter BMP), this outflow lies in one of the star-forming cores of the Perseus molecular complex, at a distance of 350 pc (Borgman & Blaauw 1964). It extends ~0.8 pc in length and has a length-to-width ratio of ~8 at the lowest velocities and more than 15 at extreme speeds. Its exciting star, IRAS 03282+3035, is highly obscured and lies embedded in a dense core that was also mapped, at low resolution, by BMP. These authors find the ammonia line shifts in velocity by 0.3 km $s^{-1}$ across the core, and they associate this shift to the effect the bipolar outflow has on the dense gas. Here, with high-resolution ammonia data, we study the interaction between this outflow and its core.

## 2. OBSERVATIONS

We observed the (1, 1) and (2, 2) transitions of ammonia using the VLA of the NRAO[3] during the night of 1992 September 4. The array was in its D configuration, with antenna spacings ranging from 2.5 to 78.9 k$\lambda$ ($\lambda$ = 1.3 cm). The two transitions were observed simultaneously and, for each of them, both polarizations were independently detected and added later. The frequency resolution, after on-line Hanning smoothing, was 24.4 kHz (0.31 km $s^{-1}$), and the total frequency coverage was 1.56 MHz (20 km $s^{-1}$). This bandwidth was wide enough to include the main and inner satellite components of $NH_3(1, 1)$ and the main component of $NH_3(2, 2)$.

The observations consisted of 15 minute integrations on IRAS 3282 interspersed with 3 minute integrations on 0333+321 to provide phase calibration. In addition, 3C 84 and 3C 48 were observed at the beginning, middle, and end of the run to provide, respectively, passband and absolute calibration. The data were edited and calibrated with the AIPS software, assuming a flux of 1.08 Jy for 3C 48.

In spite of using the VLA in its most compact configuration, an important part of the extended structure was filtered out. As only antenna spacings larger than the dish diameter (25 m) are possible, most of the flux in the spatial components larger than 50″ was lost during the observation and cannot be recovered by the usual deconvolution algorithms (CLEAN, maximum entropy, etc.). To add the missing spatial frequencies, we have used the single-dish (100 m Effelsberg telescope) ammonia data of BMP, that cover an area similar to the primary beam of the VLA antennas (~2′). The combination was carried out using the MIRIAD software (Wright & Sault 1991), following a method similar to that explained by Vogel et al. (1984). The single-dish spectra were resampled to the (lower) velocity resolution of the VLA data, deconvolved from the 100 m beam (40″), and multiplied by the VLA antenna pattern. The result was Fourier transformed and sampled randomly, generating

[1] Astronomy Department and Radio Astronomy Laboratory, University of California at Berkeley, 601 Campbell Hall, Berkeley, CA 94720.
[2] Centro Astronómico de Yebes (IGN). Apartado 148, E-19080, Guadalajara, Spain.
[3] The National Radio Astronomy Observatory is operated by Associated Universities, Inc., under cooperative agreement with the National Science Foundation.

visibilities at the low spatial frequencies that were missed by the interferometer. Comparison of the *u-v* data from the single dish and the VLA at the same spatial frequencies showed that the VLA visibilities were offset in velocity by half a channel with respect to the single-dish data. After correcting for this offset, the VLA visibilities and those derived from the single-dish spectra were combined channel by channel and Fourier transformed to generate maps. Special care was taken to ensure the calibrations of the single dish and the interferometer were consistent, and several tests were performed to check that the final maps were free from artifacts due to the data combination. The maps we present here were made using natural weighting, with a taper that produced a final beam of 8".7 × 8".2 (P.A. = 86°), and then CLEANed.

## 3. RESULTS

### 3.1. *The Ammonia Core*

Figure 1 shows the distribution of integrated $NH_3(1, 1)$ intensity (gray scale and thin contours) together with the contours of red and blue $^{12}CO(2–1)$ from BMP. The high-velocity $^{12}CO$ traces the bipolar outflow and is concentrated in two lobes that emerge from IRAS 3282, in the middle of the map, and extend SE (blue gas) and NW (red gas). The lobes are highly collimated and have little overlap; the accelerated CO has a minimum at the position of the *IRAS* source. $NH_3(1, 1)$, on the other hand, reaches its maximum toward the *IRAS* object, where it forms a compact component at the center of the outflow. From this component, two elongated extensions develop, one to the SW and the other to the north, surrounding the red lobe and highlighting its boundary. As we will see in § 4.1, these extensions correspond to enhancements in the column density. This fact, together with the elongated shape and location along the outflow edge, suggest the extensions result from the limb brightening of a shell of dense gas that surrounds the red lobe. This shell seems to be conical, with its vertex on the *IRAS* source, its axis along the red outflow, and an opening angle of ~90°. Its interior must be relatively free of dense gas in order to produce the center-to-limb contrast we observe.

The $NH_3(2, 2)$ emission, on the other hand, is much weaker. The VLA maps (not presented here) show $NH_3(2, 2)$ is only detected toward the central component and extends over ~20", like $NH_3(1, 1)$ does. Because of their lower signal-to-noise ratio, the VLA $NH_3(2, 2)$ data were not combined with single-dish observations. The $NH_3(2, 2)$ VLA-only brightness temperature towards the central component is 2 K.

### 3.2. *Velocity Structure*

In Figure 2 we present a series of velocity maps that cover the range over which we have detected $NH_3(1, 1)$. Despite the very narrow ammonia lines (everywhere ~0.5 km s$^{-1}$ FWHM, after deconvolving for hyperfine structure), the dense gas is not quiescent and has an appreciable velocity structure. The central condensation and the ammonia extensions have different kinematics.

The central condensation seems stationary ($V_{LSR}$ = 7.13 km s$^{-1}$) and its shape does not change significantly from one velocity map to the other. It is almost round, with a diameter of ~22" (7700 AU), and its proximity to IRAS 3282 suggests it represents the density enhancement that gave rise to the YSO. Its center, however, has an offset from the nominal *IRAS* position of ~8" both north and east, similar to the offset found for the submillimeter continuum peak (André & Cabrit, private communication), and compatible with the error in the *IRAS* error ellipse. Unfortunately, we cannot estimate the exact distance of the YSO to the ammonia peak from our continuum data, as no 1.3 cm flux was detected (<1 mJy). If the YSO is displaced from the *IRAS* position by the quoted amount, it will not only coincide with the ammonia and submillimeter peaks, but it will also lie at the geometrical center of the outflow.

In contrast to the quiescent central condensation, the

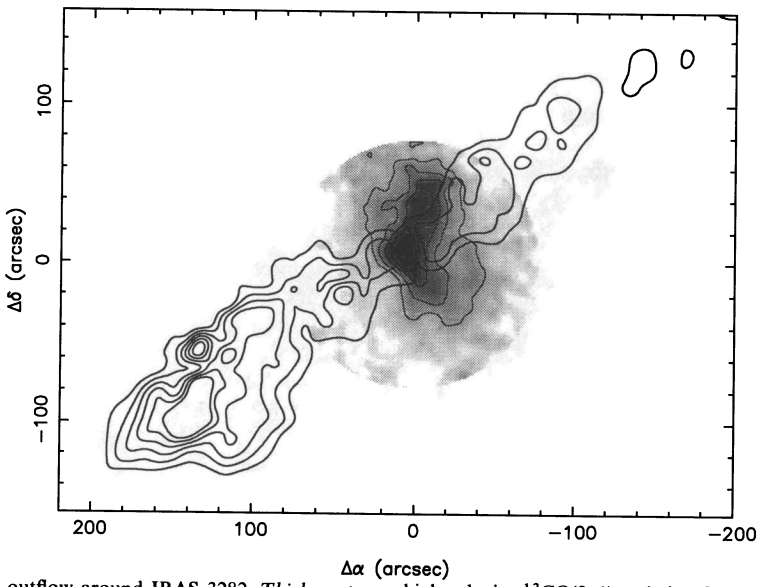


FIG. 1.—Dense core and bipolar outflow around IRAS 3282. *Thick contours*: high-velocity $^{12}CO(2–1)$ emission from Bachiller et al. (1991). The NW lobe is composed of redshifted gas ($V_{LSR}$ from 14 to 74 km s$^{-1}$), while the SE lobe contains blueshifted gas (−60 to 0 km s$^{-1}$). Contours are 9, 18, ..., 54 K km s$^{-1}$. *Gray scale and thin contours*: $NH_3(1, 1)$ integrated intensity from 6.5 to 8 km s$^{-1}$. Contours are 2, 3, ..., 6 K km s$^{-1}$. The $NH_3(1, 1)$ emission has been corrected for the attenuation by the primary beam of the VLA antennas (FWHM = 112"), and only the region where the attenuation was less than 0.25 is shown. The coordinates are referred to the position of IRAS 03282+3035 [$\alpha$(1950) = 03$^h$28$^m$15$^s$.2, $\delta$(1950) = 30°35'14"].

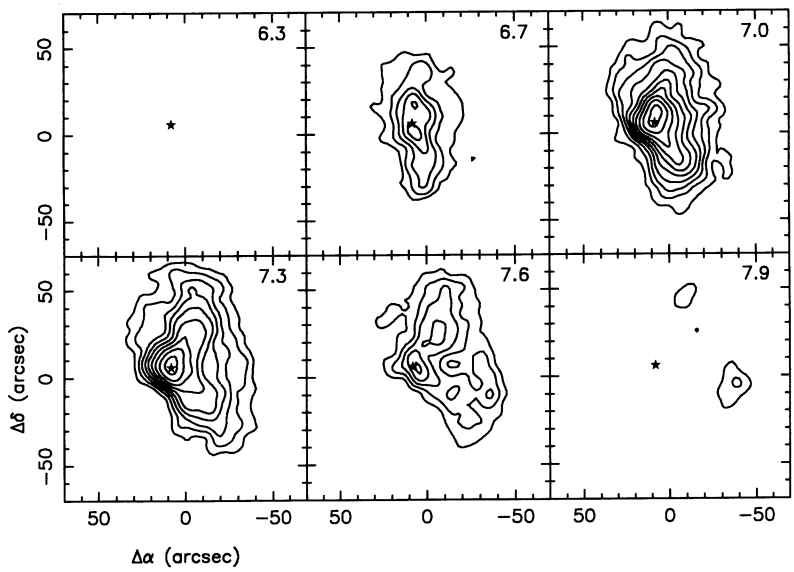


FIG. 2.—Channel maps of the $NH_3(1, 1)$ emission for the velocity range with detected intensity. The central velocity of each channel is indicated in the upper right corner. Channel width is 0.31 km $s^{-1}$. Contours are 1, 1.6, 2.2, ..., 6.4 K. No primary beam correction was applied because of the lower signal-to-noise of the data. Coordinates have the same origin as in Fig. 1. The star represents the position of the submillimeter continuum peak from André & Cabrit (private communication).

ammonia extensions present a systematic velocity field. At the bluest velocities ($V = 6.7$ km $s^{-1}$ panel), both extensions are aligned north-south. As the gas gets redder (panels 7.0 and 7.3 km $s^{-1}$), the southern extension moves from south to southwest, and the northern extension becomes more prominent and oriented slightly northwest. At $V = 7.6$ km $s^{-1}$ the extensions fully surround the red CO lobe and form a distribution with the shape of a "U". Finally, at the reddest velocities (7.9 km $s^{-1}$ map), the emission peaks at the end of the extensions, suggesting that the velocity of the dense gas increases with distance from the *IRAS* source.

The systematic change in the position angle of the extensions results from the dense gas getting redder as it lies closer to the red CO outflow. This pattern resembles a shear flow in a pipe, where the fastest gas runs along the center and its velocity decreases toward the walls. The analogy, in fact, seems appropriate for the IRAS 3282 outflow, as there is a global trend of decreasing velocity with increasing distance from the axis. The maps of BMP show the very fast CO ($\sim$60 km $s^{-1}$) forms a narrow, highly collimated jet that runs along the outflow center. As the velocity decreases, the jet grows wider, until at $\sim$20 km $s^{-1}$, the red gas fills the ammonia cavity. Because of the high optical depth of CO, BMP could not study the lowest velocity regime of the outflow and could not see, as we do now with ammonia, that the velocity trend continues all the way to almost zero velocity. This continuity in the velocity field from the hypersonic $^{12}CO$ to the slowly moving ammonia shows the red outflow is accelerating the dense gas as it travels through the core, and it also suggests the high-velocity gas is responsible for evacuating the ammonia cavity. Both the shear pattern and the cavity along the red lobe seem to result from the acceleration of the dense gas by the highly collimated outflow.

## 4. DISCUSSION

### 4.1. *Physical Conditions of the Dense Gas*

To estimate the ammonia column density and the total mass of the core, we have derived the $NH_3(1, 1)$ optical depth from the spectra by fitting, at each position, the main and two innermost hyperfine components in a similar way to that described by Pauls et al. (1983). The optical depths range from 1 to 3 over most of the core and have a spatial distribution resembling that of the integrated intensity, with the central condensation and the ammonia extensions having twice the optical depth of the valley along the red CO outflow. These higher optical depths, together with the higher brightness temperatures, can only occur if the extensions are regions where the $NH_3$ column density is twice as large as in the valley between them, a result that reinforces the idea that extensions arise from limb-brightened shells that surround the outflow. The high optical depths ($\tau_m > 1$), in fact, mitigate the brightness contrast that would be expected if the emission were optically thin.

The central condensation, in addition to strong $NH_3(1, 1)$ emission, has detectable $NH_3(2, 2)$, and from the two intensities we estimate a kinetic temperature of 12 K. This temperature, together with the optical depth derived from the fit ($\tau_m = 3.1$), implies a total ammonia column density of $1.3 \times 10^{15}$ $cm^{-2}$. If we use the ammonia abundance derived by BMP from single-dish observations ($9 \times 10^{-8}$), we derive an $H_2$ column density of $1.4 \times 10^{22}$ $cm^{-2}$. This value, however, seems too low, as it corresponds to a visual extinction of only 14 mag, in apparent contradiction with the nondetection of IRAS 3282 by Aspin (1992) at 2 $\mu$m, who suggests an extinction larger than 50 mag. The ammonia abundance in the core must therefore be lower than that derived by BMP, and our $H_2$ column density should be considered a lower limit.

If we assume the central condensation is spherical with diameter of 7700 AU (§ 3.2), we estimate a minimum mass of 0.36 $M_\odot$ from the $H_2$ column density. To estimate the total mass of the core, we assume the kinetic temperature is also 12 K. This assumtion is supported by the single-dish measurements of BMP, who derive the same temperature in a 40″ beam as we derive in our 8″ beam, an indication that the temperature is almost constant across the core. With this value, we convert the optical depth at every point into an ammonia column density, and using the same abundance as before, we derive a mass of 2 $M_\odot$, in good agreement with the estimate of BMP.

The central condensation, therefore, contains ~20% of the mass in the core.

### 4.2. *Core and Outflow Asymmetries*

The CO outflow from IRAS 3282 is not symmetric. Figure 1 shows the red lobe is weaker than the blue lobe, and BMP estimated there is 0.6 times less red gas than blue gas. This difference in mass corresponds to a difference in momentum of 0.24 $M_\odot$ km s$^{-1}$. It is unlikely, however, that there is an intrinsic momentum asymmetry between the two lobes of the outflow, as this would imply the flow exerts a net force on the star. It is more likely that the observed asymmetry results from an incomplete momentum account.

The core around IRAS 3282 is also asymmetric. Despite the small uncertainty in position, clearly the YSO does not lie at the centroid of the dense gas but near the east boundary (Fig. 1); although the star coincides with the ammonia peak, most of the emission extends toward the west. It seems tempting to relate the asymmetry of the CO outflow with the asymmetry of the dense gas, as the CO maps show there is more low-density, high-velocity gas towards the east, while the ammonia maps show there is more high-density, low-velocity gas toward the west. In order to explain the observed anticorrelation between CO and $NH_3$ we propose the following scenario: if the highest density peak of the core was offset toward the east, the star that formed inside of it was surrounded by different amounts of dense gas in different directions. When this star excited a bipolar outflow, the high-velocity gas in each lobe encountered a different resistance in each direction. The blue outflow, moving toward the east, had little dense gas in its way and could flow unimpeded. The red outflow, moving toward the west, encountered more dense gas and slowed down, transferring part of its momentum to the dense gas. The asymmetry between the CO lobes of Figure 1 would therefore result not from an intrinsic asymmetry of the outflow, but from the fact the blue lobe is mostly composed of fast gas, while the red lobe contains a larger fraction of slow gas. When the outflow is observed in CO, only the high-velocity gas is traced (the slow red gas is confused with the ambient cloud) and the blue lobe is artificially enhanced. It is only when we study the low-velocity regime, with $NH_3$ for example, that we find part of the missing momentum in the form of a shear flow of dense gas. Therefore, it is possible that both lobes have equal momenta, and that the differences in the CO maps arise just from their different distribution in velocity. The asymmetry of the outflow may just reflect the asymmetry of the core.

Despite traveling through different environments and suffering different decelerations, both CO lobes have similar collimation (see Fig. 1 and BMP's Fig. 7). If the asymmetry of the core does not to affect the collimation, the mechanism that maintains it must be rather robust. An underlying jet seems a likely candidate, given the very high collimation of the accelerated CO. It is not clear, though, whether the fastest CO traces the proper jet or it resuls from gas swept up by an underlying invisible jet, even faster and more collimated. Perhaps the shear pattern we observe extends to even higher velocities than those traced by CO. The study of shear in molecular outflows appears as a promising tool to reveal the presence of these underlying jets, and to understand the mechanism that accelerates the molecular gas.

We thank the VLA staff for their support during the observations and data calibration. We also thank Matthew Richter for his careful reading of the manuscript. M. T. and M. C. H. W. were partially supported by the NSF grant AST 91-00307.

REFERENCES

Aspin, C. 1992, A&A, 266, 416
Bachiller, R., & Gómez-González, J. 1992, Astron. Astrophys. Rev., 3, 257
Bachiller, R., Martín-Pintado, J., & Planesas, P. 1991, A&A, 251, 639 (BMP)
Borgman, J., & Blaauw, A. 1964, Bull. Astron. Inst. Netherlands, 17, 358
Lada, C. J. 1985, ARA&A, 23, 267
Myers, P. C., Heyer, M., Snell, R. L., & Goldsmith, P. F. 1988, ApJ, 324, 907
Pauls, T. A., Wilson, T. L., Bieging, J. H., & Martin, R. N. 1983, A&A, 124, 23
Shu, F. H., Adams, F. C., & Lizano, S. 1987, ARA&A, 25, 23
Snell, R. L. 1987, in IAU Symp. 115, Star-forming Regions, ed. M. Peimbert & J. Jugaku (Dordrecht: Reidel), 213
Umemoto, T., Hirano, N., Kameba, O., Fukui, Y., Kuno, N., & Takakubo, K. 1991, ApJ, 377, 510
Vogel, S. N., Wright, M. C. H., Plambeck, R. L., & Welch, W. J. 1984, ApJ, 283, 655
Wright, M. C. H., & Sault, R. J. 1991, in IAU Colloq. 131, Radio Interferometry: Theory, Techniques, and Applications, ed. T. J. Cornwell & R. A. Perley (ASP Conf. Ser.) (San Francisco: ASP), 276